RESEARCH ARTICLE | JULY 22 2024

Charge transfer plasmons in nanoparticle arrays on graphene: Theoretical development

Special Collection: Plasmonics and Optical Metastructures

A. S. Fedorov ✉ ⓘ ; E. V. Eremkin ⓘ

Check for updates

View Online   Export Citation

Charge transfer plasmons in nanoparticle arrays on graphene: Theoretical development

View Online   Export Citation   CrossMark

A. S. Fedorov[1,2,a)] (ID) and E. V. Eremkin[2,b)] (ID)

AFFILIATIONS

[1]Kirensky Institute of Physics, Federal Research Center KSC SB RAS, Krasnoyarsk 660036, Russia
[2]International Research Center of Spectroscopy and Quantum Chemistry—IRC SQC, Siberian Federal University, Krasnoyarsk 660041, Russia

Note: This paper is part of the special topic, Plasmonics and Optical Metastructures.
[a)]**Author to whom correspondence should be addressed:** qchem99@yandex.ru
[b)]**Electronic mail:** eremkin.e.v@yandex.ru

ABSTRACT

The properties of charge transfer plasmons (CTPs) in periodic metallic nanoparticle arrays (PMNPAs) on the single-layer graphene surface are studied within a computationally efficient original hybrid quantum-classical model. The model is based on the proven assumption that the carrier charge density in doped graphene remains unchanged under plasmon oscillations. Calculated CTP frequencies for two PMNPA geometries are shown to lie within the THz range and to be factorized, i.e., presented as a product of two independent factors determined by the graphene charge density and the PMNPA geometry. Equations are derived for describing the CTP frequencies and eigenvectors, i.e., oscillating nanoparticle charge values. It is shown that the CTP plasmons having a band structure containing a wave vector and a band number, like to phonons in periodic media, can be divided into an acoustic mode and optical CTP modes. For the acoustic modes, the CTP group velocity tends to zero at $k \to 0$, but reaches a value of $\sim V_{\text{Fermi}}$ in graphene inside the Brillouin zone, while for the optical modes, the group velocity dispersion is extremely weak, although their energy is higher than the acoustic plasmon energies. It is shown that the calculated dependence of CTP frequencies on the carrier concentration in graphene is in good agreement with experimental data. We believe that the proposed model can help in designing various graphene-based terahertz nanoplasmonic devices of complex geometry due to very high computational efficiency.

I. INTRODUCTION

Terahertz (THz) radiation lies between the infrared (IR) and microwave ranges and typically covers the frequencies from 300 GHz to 30 THz, which correspond to the wavelengths from 1 mm to 30 μm. Recent advances in nanotechnology and photonics demonstrated the high application potential of THz technology for various fields.[1] A unique feature of THz radiation is its ability to penetrate with minimum losses through the materials (plastic, paper, clothing, wood, etc.) that are normally opaque to visible light. Due to the remarkable rotational and vibrational resonances of molecules at THz frequencies, this radiation can detect a multitude of molecules.[2] Today, THz technology finds application in the detection of explosives and drugs, security checks, spectroscopy, image transmission, biomedical research,[3] food quality control, environmental monitoring,[4] and

many other areas. Terahertz devices used in nondestructive testing are safe for humans, in contrast to x rays.

The most efficient current THz spectroscopy and visualization systems combine photoconductive antennas with femtosecond lasers generating THz waves.[5] However, fast laser sources included in these systems make them bulky, expensive, and high-maintenance.

Recent studies underscore the potential of graphene for some applications, in particular, THz optoelectronics. As was demonstrated in Ref. 6, graphene plasmons or rather graphene plasmon polaritons (GPPs) with their high performances can replace noble metal plasmons. These features make graphene a perfect material for creating plasmonic devices. Its main advantage is related to the unique band structure, which spans the THz and IR ranges.[7–9] At the same time, due to difference the in the speeds of photons and plasmons in graphene, the high-efficiency energy transfer from the

electromagnetic radiation to graphene is a challenge. Therefore, various graphene-based metamaterials are used to match these speeds. To enable the direct coupling of GPP and free-space radiation, different surface gratings, such as periodical ribbons[10] or disks,[11] have been used. The grating allows us to eliminate the requirement of in-plane momentum conservation.

In recent years, some works have appeared devoted to properties of 2D metamaterials consisting of regular arrays of metallic nanoparticles (NPs) on various dielectric substrates. In Ref. 12 by the coupled dipole (CD) method, it was numerically obtained a narrow localized surface plasmons (LSPs) extinction peaks in the 1D silver nanoparticle array that is explained by the interaction of LSP in individual NPs.

In Refs. 13 and 14, it was shown that the presence of a dielectric substrate under metal NPs entails the interaction of LSPs and diffractive grating Rayleigh anomalies. This interaction leads to the generation of lattice resonances having high quality factors Q ($\approx$ 2340, see Ref. 14) throughout the visible spectral ranges. Unfortunately, since the frequency of LSPs in metal NPs lies in the visible or near-infrared range, it is impossible to obtain plasmon frequencies in the THz range in such systems.

Recently, various metamaterials for different THz applications have been also proposed. In Ref. 15, it was reported a metamaterial, which comprises T-shaped gold elements combined with a graphene layer. This compound exhibited high absorption in the range of 20.8–39.7 THz. In Ref. 16, a polarizer based on graphene and a gold resonator grid was explored. This device had a negative effective refractive index and was stable across different beam incidence angles. Wang et al.[17] investigated hybrid metal–graphene metastructures consisting of arrays of split gold periodic rods over a graphene monolayer. These structures allowed the THz transmission modulation by the gate voltage. Liu et al.[18] introduced a multi-layered metamaterial based on metal and graphene layers promising for broadband applications. The use of graphene with concentric hexagonal-shaped gold rings was described in Ref. 19, and the possibility of precise tuning of resonance frequencies in the THz range was demonstrated. Finally, Wu et al.[20] proposed a dynamic THz absorber made of graphene with gold nanostrips.

In Ref. 21 (see Fig. 1), the authors created a regular square-periodic array of gold nanocylinders on graphene where GPP absorption features were measured. It was possible to effectively manage GPP resonances across the 2–8 THz range by changing the array period or changing the doping of graphene.

The cited works opened new avenues for the development and application of THz optoelectronic devices. Unfortunately, in many of these works (see, e.g., Refs. 10, 11, and 21), plasmon frequencies were calculated using a simplified formula,[22] which included the properties of only graphene and its coverings,

$$k(\omega) = \frac{\pi\hbar^2\varepsilon_0(\varepsilon_{r1} + \varepsilon_{r2})}{q^2 E_f}\left(1 + \frac{i}{\omega\tau}\right)\omega^2, \qquad (1)$$

where $k(\omega)$ is the in-plane wavevector of the GPP, ε_0 is the vacuum permittivity, ε_{r1} and ε_{r2} are the dielectric constants of the materials above and below the graphene film, τ is the carrier scattering time, and E_f is the Fermi energy measured from the Dirac point, wherein
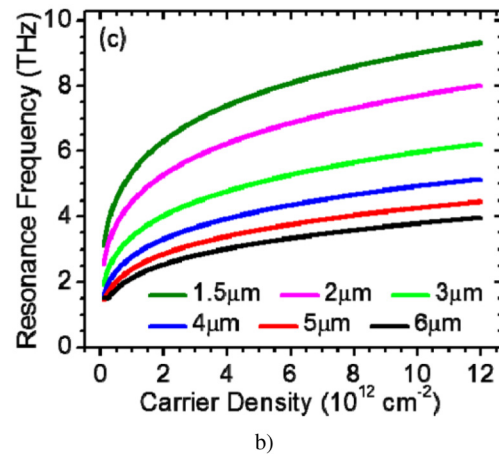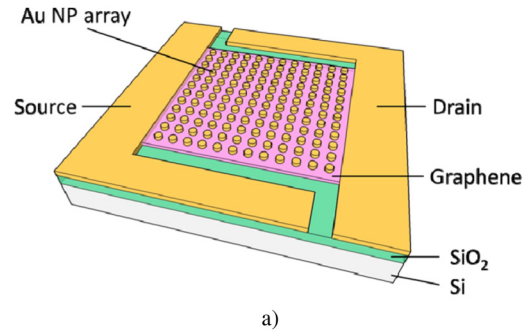
a)

b)

FIG. 1. (a) Schematic illustration of the PMNPA on graphene. (b) Resonance frequency of graphene plasmon polaritons, plotted as a function of carrier density ρ for different values of period.[21] Reproduced with permission from Tantiwanichapan *et al.*, ACS Photonics **4**, 2011 (2017). Copyright 2017 American Chemical Society.

the geometric characteristics of nanoobjects (disks, strips, etc.) on the graphene surface remained outside of consideration, although they should influence the GPP spectrum. A full consideration of these characteristics should lead to very complex equations derived in the optics of surface gratings (see, e.g., Ref. 23).

At the same time, there are commercial electromagnetic solvers based on Finite Element Method (FEM) or Finite Difference Time Domain (FDTD) methods, based on numerical discretization of the electromagnetic field.[24,25] They allow to find plasmonic excitations for systems with any given geometry.[26–28] Unfortunately, calculations of charge transfer plasmon (CTP) frequencies by these methods for complex 3D-systems having many connected nanoparticles are very time consuming. At the same time, the calculations of the CTP frequencies of complex systems using the model we develop here take 3–4 orders of magnitude less time.

The purpose of this work is to consider the spectrum of GPP based on a completely different model—on the concept of CTP plasmons, which arise when periodic metal nanoobjects are placed on the graphene surface. These equations can be very simple but allow to calculate the CTP plasmon spectrum for complex systems containing metal nanoparticles periodical array on the graphene surface.

In this study, we develop our previous hybrid quantum-classical model, which was first used to describe CTPs in systems of metal NPs linked by narrow conductive molecular bridges, where quantum effects are expected to be quite substantial.[29–31] Recently, we have used it to describe CTPs in irregular arrays of metal NPs on graphene, which was very numerically efficient.

II. QUANTUM-CLASSICAL MODEL OF CTPs FOR PMNPAs ON GRAPHENE

Here, we extend our previous model[35] to calculate properties of CTP plasmons to systems included periodic metallic nanoparticle arrays (PMNPAs) on graphene. As the main equation, for these systems, we use again the total energy conservation law,

$$\frac{dE_{tot}}{dt} = \frac{dE_{pot}}{dt} + \frac{dE_{kin}}{dt} = 0, \tag{2}$$

where the potential energy $E_{pot} = E_{NP}$ is the electrostatic energy of charged NPs and the kinetic energy $E_{kin} = E_{graphene}$ is the energy of moving carriers in graphene.

In the previous model, we have proven several points. First, it was proved the changes in the graphene carrier density can be neglected during CTP vibrations, wherein the redistribution of the carriers density inside NPs can also be neglected because of the change that occurs during NP localized surface plasmon (LSP) excitation, which frequencies lie in the vis frequency range, which is much higher than THz frequencies. Second, we have demonstrated that the CTP energy losses consisting of energy losses in graphene and in the NPs are quite small, so the total quality factors Q of CTP plasmons in NPs–graphene systems are $Q \sim 10$–100. Third, calculations of the total transmittance T of the NPs–graphene interface using the nonequilibrium Green function (NEGF) method[33] have shown that the NPs–graphene contact resistance can be neglected, so we will neglect this effect below.

Now, to build the model describing the properties of CTP plasmons in regular arrays of metal NPs on graphene, we assume several points. First, for simplicity, the radius of all NPs is equal to R and each NP–graphene has a contact spot of radius R_0, through which the NP charge flows to graphene. Second, due to periodicity and by analogy with phonons in a periodic media, it is assumed the CTPs are characterized by the wave vector $\vec{k}$ and the band number n. Therefore, in the CTP plasmon with band number n and frequency ω_n, the NP charges $Q_{j,n}$ would be changed harmonically,

$$Q_{j,n}(\vec{R}_j, t) = Z_{j,n}(\vec{R}_j)e^{i\omega_n t}, \tag{3}$$

where $Z_{j,n}(\vec{R}_j)$ is the charge amplitude for the NP having the coordinate $\vec{R}_j$ and the band index n. The current from the NP to graphene, equal to $\dot{Q}_j$ would be changes harmonically as well. Using Bloch's theorem, the NP charge amplitude $Z_{j,n}$, having the wave vector $\vec{k}$ and the band number n but lying in another unit cell (UC) with the translation vector $\vec{R}_n$ would be changed harmonically,

$$Z_{j,n}(\vec{R}_j + \vec{R}_n) = Z_{j,n}(\vec{R}_j)e^{i\vec{k}\vec{R}_n}. \tag{4}$$

Third, the time derivative of the density of the kinetic energy of carriers in graphene is determined by the work of external
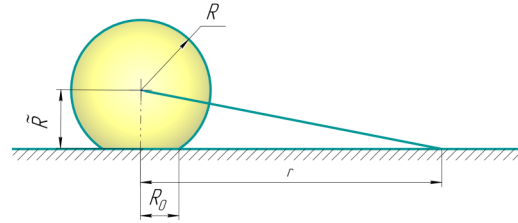

FIG. 2. NP on graphene: r is the radius vector in the graphene plane, R is the NP radius, and θ is the angle between r and the radius of the vector coming out of the NP center.

electric forces acting on these carriers[34] taken with the opposite sign,

$$\frac{dE_{kin}}{dt} = -\frac{1}{2}j(r)E^*(r) = -\frac{\sigma(\omega, \mu)}{2}\int_\Omega E(r)E^*(r)$$
$$= -\frac{1}{2}\sigma(\omega, \mu)\int_\Omega \nabla_\parallel\left(\varphi(r)\nabla_\parallel\varphi^*(r)\right)d^2r, \tag{5}$$

where $\sigma(\omega, \mu, T)$ is the graphene conductivity, depending on the graphene chemical potential μ, temperature T, and frequency ω, and $\varphi(r)$ is the electric potential at point r on graphene and $\nabla_\parallel$ is the parallel to the graphene plane component of the gradient.

As was obtained in Ref. 35, only intraband Drude contribution $\sigma_{intra}(\omega, E_f) = \frac{e^2 E_f}{\pi \hbar^2}\frac{i}{\omega + i\tau^{-1}}$ is essential in the THz range, wherein $\tau \sim 10^{-13}$ s is the graphene free carrier momentum relaxation time and it affects the CTP quality factor factors.

Taking into account the periodic boundary conditions (PBCs) [see (4)] and assumption that the graphene charge density does not changed under the plasmon oscillations, the Coulomb potential $\varphi(r)$ in the graphene is equal to the double sum of the potentials induced by charged NPs j inside UC and over all UCs with index n,

$$\varphi(r) = \sum_{j=1,n}^{N}\frac{Z_j(\vec{R}_j)e^{i\vec{k}\vec{R}_n}}{|\vec{r} - (\vec{R}_j + \vec{R}_n)|}$$
$$= \sum_{j=1,n}^{N}\frac{Z_j e^{i\vec{k}\vec{R}_n}}{8\pi^3}\int_q \Phi_{coul}(q)e^{i\vec{q}(\vec{r} - \vec{R}_j + \vec{R}_0)}d^3q, \tag{6}$$

where N is the number of NPs inside UC, n is the UC index, and the Fourier image of the Coulomb potential $\Phi_{coul}(q) = \frac{4\pi}{q^2}$. Here, we should keep in mind that the center of NPs is raised over the graphene plane (see Fig. 2).

While calculating $\varphi(r)$, it is convenient to enter the parallel ($q_\parallel$) and transverse (q_z) to the graphene plane components of the reciprocal space vector $\vec{q}$. After this, (6) can be rewritten as

$$\varphi(r) = \sum_{j,n}\frac{Z_j e^{i\vec{k}\vec{R}_n}}{2\pi^2}$$
$$\times \int_{q_\parallel, q_z}\frac{e^{-i\left(\vec{q}_\parallel(\vec{r} - (\vec{R}_j + \vec{R}_n)) + q_z\widetilde{R}\right)}}{q_\parallel^2 + q_z^2}dq_z d^2q_\parallel, \tag{7}$$

where $\vec{k}$ is the plasmon wave vector and $\widetilde{R} = \sqrt{R^2 - R_0^2}$ is the distance from the NP center to the graphene surface (see Fig. 2).

Since we are interested in the potential component $\varphi_\parallel$, acting only in the graphene plane, we can integrate Eq. (7) over all the q_z values and obtain the Fourier image of the potential Φ acting in the plane,

$$\Phi(q_\parallel) = \int_{-\infty}^{\infty} \frac{4\pi}{q_\parallel^2 + q_z^2} e^{-iq_z \widetilde{R}} dq_z. \tag{8}$$

Therefore, the potential $\varphi(r)$ in the graphene plane can be calculated as

$$\varphi(r) = \sum_{j,n} \int_{q_\parallel} \frac{Z_j e^{i(\vec{k}+\vec{q}_\parallel)\vec{R}_n}}{(2\pi)^3} \Phi(q_\parallel) e^{-i\vec{q}_\parallel(\vec{r}-\vec{R}_j)} d^2 q_\parallel, \tag{9}$$

using the lattice sum, $\sum_n e^{i(\vec{k}+\vec{q}_\parallel)\vec{R}_n} = \frac{(2\pi)^2}{\Omega_0} \sum_{\vec{G}} \delta(\vec{k}+\vec{q}_\parallel, \vec{G})$, where Ω_0 is the unit cell area and $\vec{G}$ are the planar reciprocal lattice vectors; the potential $\varphi(r)$ becomes equal,

$$\varphi(r) = \sum_{j,\vec{G}} \frac{Z_j \Phi(\vec{G}-\vec{k})}{2\pi\Omega_0} e^{-i(\vec{G}-\vec{k})(\vec{r}-\vec{R}_j)}. \tag{10}$$

From this equation, it is easy to obtain $\nabla_\parallel \varphi(r)$ in (5). Applying another sum rule $\int_\Omega e^{i(\vec{G}_2-\vec{G}_1)\vec{r}} d^2 r = \Omega_0 \delta(\vec{G}_1 - \vec{G}_2)$, one can transform Eq. (5) as

$$\frac{dE_{kin}}{dt} = \frac{\sigma(\omega,\mu)}{16\pi^2\Omega_0} \sum_{j,i} Z_j^* Z_i \times$$
$$\times \sum_G |\Phi(G-q)|^2 e^{i(\vec{k}-\vec{G})(\vec{R}_j-\vec{R}_i)}(\vec{k}-\vec{G})^2$$
$$= \frac{\sigma(\omega,\mu)}{2} \sum_{i,j} B_{i,j}(\vec{k}) Z_j^* Z_i, \tag{11}$$

where the kinetic energy matrix is

$$B_{i,j}(\vec{k}) = \frac{\sigma(\omega,\mu)}{8\pi^2\Omega_0} \sum_G |\Phi(G-k)|^2 e^{i(\vec{k}-\vec{G})(\vec{R}_j-\vec{R}_i)}(\vec{k}-\vec{G})^2.$$

In addition, we can calculate the potential energy of the unit cell as

$$E_{pot} = \sum_{i \in 1} \left(\frac{Q_i \varphi(R_i)}{2} + \frac{Q_i^2}{2R} \right).$$

By analogy with the kinetic energy calculation, one can calculate the potential energy of the unit cell as

$$E_{pot} = \sum_{i,j \in 1} \frac{Q_j Q_i}{4\pi\Omega_0} \sum_G \Phi_{coul}(\vec{G}-\vec{k}) e^{-i(\vec{G}-\vec{k})(\vec{R}_i-\vec{R}_j)}$$
$$+ \sum_{i \in 1} \frac{Q_i^2}{2R} = \sum_{i,j} A_{i,j}(\vec{k}) Q_j^* Q_i, \tag{12}$$

where the potential energy matrix is

$$A_{i,j}(\vec{k}) = \frac{\delta_{i,j}}{R} + \sum_{i \neq j} \frac{2}{|R_i - R_j(\vec{k})|}$$
$$= \frac{\delta_{i,j}}{R} + \sum_{\vec{G}} \frac{\Phi_{coul}(\vec{G}-\vec{k})}{4\pi\Omega_0} e^{-i(\vec{G}-\vec{k})(\vec{R}_i-\vec{R}_j)}.$$

Using (3) and (12), the potential energy time derivative is

$$\frac{dE_{pot}}{dt} = \frac{d}{dt} \sum_{i,j} A_{i,j}(\vec{k}) Q_i Q_j^* = i\omega \sum_{i,j} A_{i,j}(\vec{k}) Z_i Z_j^*. \tag{13}$$

Using Eqs. (2), (11), and (13), we can derive the main matrix equation as

$$\sum_{i,j} \left[i\omega Z_i A_{i,j}(\vec{k}) Z_j - \sigma_{intra}(\omega, E_f) Z_i B_{i,j}(\vec{k}) Z_j \right] = 0. \tag{14}$$

Assuming that the graphene carrier dissipation processes are much less than the energies of the plasmons under study or, in other words, $\tau \to \infty$, (14) can be written in the following matrix form:

$$\alpha\omega^2 \hat{A}(\vec{k}) - \hat{B}(\vec{k}) = 0; \quad \alpha = \frac{\pi\hbar^2}{e^2 E_f}. \tag{15}$$

Introducing $\hat{W}(\vec{k}) = \hat{A}(\vec{k})^{-1} \hat{B}(\vec{k})$ and using the well-known formula for graphene $E_f = \hbar V_{fermi}\sqrt{\pi\rho}$, one can get the secular equation for determining the CTP frequencies,

$$\omega_i^2(\vec{k}) = \frac{e^2 V_{fermi}\sqrt{\rho}}{\sqrt{\pi}\hbar} \cdot \text{eigenvalues}(\hat{W}(\vec{k})). \tag{16}$$

This equation is exactly like Eq. (18) in Ref. 35 for CTPs in an irregular NP array on the graphene except that the matrix $\hat{W}(\vec{k})$ has a different form. It is clear that the CTP frequency ω_i are decomposed into factors, which are the function of carrier density in graphene and the function depending on the NP coordinates in the unit cell and the CTP wave vector only. The dependence of the matrix $\hat{W}$ on the planar vector $\vec{k}$, which is determined by the dependences of matrices $A_{i,j}(\vec{k})$ and $B_{i,j}(\vec{k})$, has symmetry determined by the planar geometry of NPs on the graphene surface.

Considering case $|k| \to 0$, taking into account the system general electrical neutrality and the assumption the changes in the graphene carrier density can be neglected during CTP vibrations, it

07 August 2024 13:54:35

becomes obvious that in this case, one acoustic and some optical CTP plasmonic modes can be existed.

For the acoustic plasmonic mode of index $n0$, the amplitudes of all NP charges $Z_{j=1...N,n0} \to 0$ when $|k| \to 0$. This leads to a zero restoring force acting on all free carriers and to the CTP frequency $\omega_{n0} \to 0$. There must also exist (N−1) CTP optical modes, where $Z_{j,n} \neq 0$ for at least some NPs inside UC. Because of this, a changing local electric field in the graphene changes the kinetic energy of carriers there, determined by the kinetic $B_{i,j}$ matrix, as well as the potential energy of charged NPs, defined by the $A_{i,j}$ potential matrix. This leads to a nonzero matrix $\hat{W}$ and to nonzero values of CTP frequencies ω_i for the optical CTP branches. The situation here is completely analogous to phonon spectra in periodic media, where acoustic and some optical vibration modes are also observed.

III. APPLICATION OF THE MODEL

We apply the developed model for two periodic systems involving metallic NPs with a radius of $R_{np} = 3$ nm placed on the graphene surface (see Fig. 3). The first structure includes a chain of four identical NPs uniformly spaced in the UC. The distance
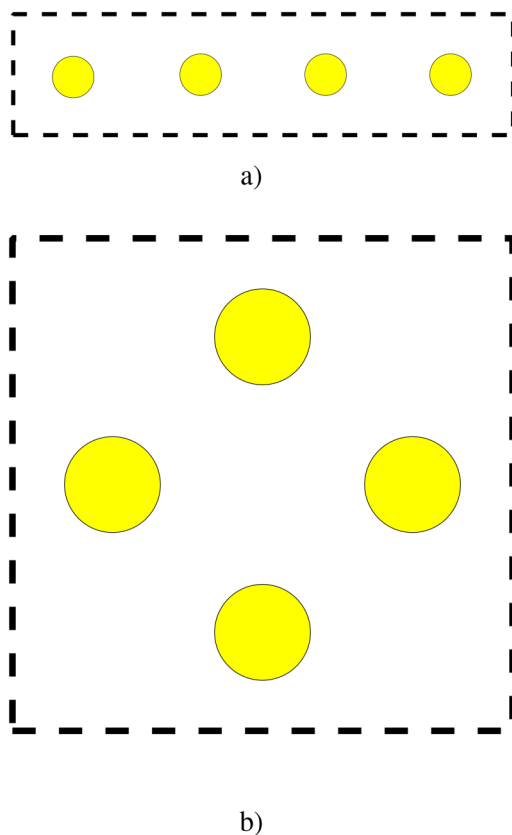

a)

b)

FIG. 3. Unit cells of two NP–graphene systems. (a) Chain structure including four NPs on graphene. (b) Square structure including four NPs on graphene. Dashed lines show the unit cell boundaries.

between the centers of neighboring NPs is $R_{neigh} = 5R$ and the parameters of a rectangular UC are $a = 20$ R and $b = 5$ R. At the same time, the UC could be reduced to the smallest primitive UC containing inside only one NP. Like phonons in a similar periodic structure, the CTP band structure for this system should lead to the bandgap absence between an acoustic and all optical modes of CTPs.

The second investigated structure [see Fig. 3(b)] included four identical NPs in the symmetrical square UC, and this UC is chosen so that it cannot be decomposed into a simpler UC. The system includes a square of four NPs inside UC with the diagonal length between the NP centers $R_{diag} = 6$ R, where the UC sides are rotated by 45 deg relative to the square sides. The parameters of the square UC are $a = b = 10$ R.

Using (16), we determined the band structures $\nu(\vec{q})$ for both NP–graphene systems [see Figs. 4(a) and 4(b)]. These modes can be divided again into the acoustic and optical CTP branches. In both structures, the CTP frequencies of the acoustic modes tend to zero as $\vec{k} \to 0$ and reach the maximum at the first Brillouin zone (1BZ) boundaries. The optical CTP modes have the weak $\nu(\vec{k})$ dispersion, although their frequencies are higher than those of the acoustic modes. In any case, the frequencies of all $\nu(k)$ modes range within 0–10 THz.

Interestingly, the first chain structure of equidistant NPs contains no bandgap between the acoustic and optical CTP modes [see Fig. 4(c)]. This can be explained by the fact that this structure can be reduced to another structure containing only one NP in the UC, where there is the only one acoustic mode. By folding, this mode is mapped onto a set of acoustic and three optical modes in the reduced UC, where the modes at the 1BZ boundaries transform into each other without forming a bandgap, similar to the situation with the acoustic branch of phonons in a crystal with only one atom in the UC.

The band structure of the second square structure has a bandgap between all CTP branches, since it cannot be reduced to the structure with the single NP inside UC. The band gaps between higher optical modes are narrow and difficult to distinguish in the figure.

It should be noted that solving of (16) on a PC with CPU Intel Core I5-3340, 3.1 GHz for one k point in 1BZ takes only a few seconds, which indicates the high computational efficiency of the developed model. Our practice[35] shows that similar calculations, but for non-periodic NP–graphene structures within the framework of the Finite Element Method (FEM) or Finite Difference Time Domain (FDTD) method, which have become the *de facto* standard for such calculations, take about a day or more on a similar computer.

For the structures under study, the plasmon group velocities denoted as $V_{group}(\vec{k}) = \frac{d\nu(\vec{k})}{dk}$ were investigated also. Figure 5 shows these velocities depending on the wave vector k_x along the x axis. For convenience, these group velocities were normalized to the Fermi velocity of electrons near the Dirac cones $V_{fermi} \simeq 10^6$ m/s. It can be clearly seen that there are certain $\vec{k}$ ranges where $V_{group}(\vec{k})$ surpasses the Fermi velocity of electrons V_{fermi}.

Next, the dependence of the CTP frequencies for both systems on the graphene carrier concentration $\rho(1/\text{cm}^2)$ was calculated and plotted (see Fig. 6), wherein NP radius $R = 375$ nm and the cell
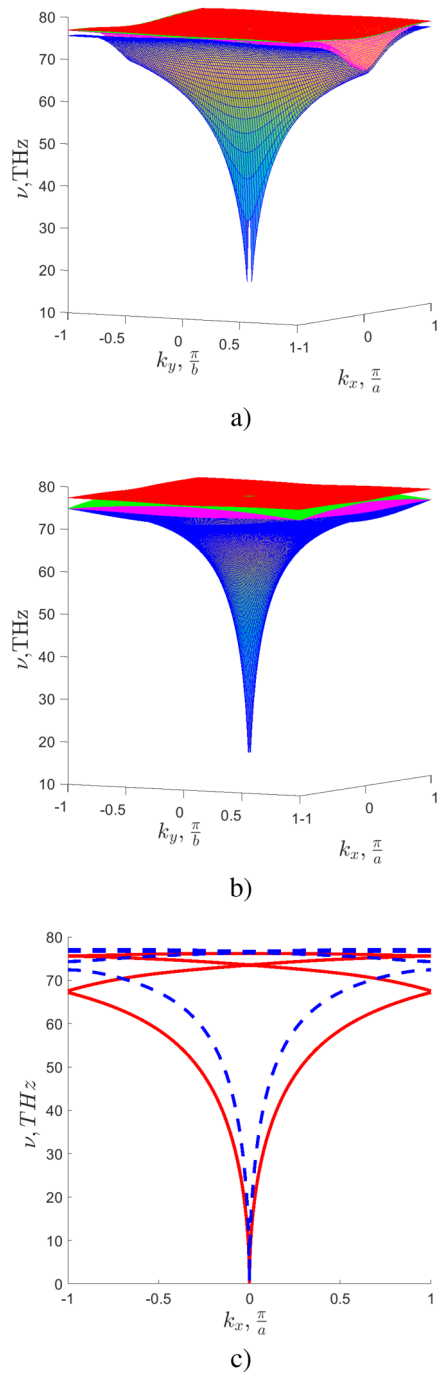
07 August 2024 13:54:35

a)

b)

c)

FIG. 4. (a) Band structure $\nu(\vec{k})$ for the UC included the chain of four NPs on graphene; (b) $\nu(\vec{k})$ for the structure of four NPs in the square UC; (c) cross section of $\nu(\vec{k})$ on k_x with $k_y = 0$ for both structures. The red solid line corresponds to (a); the blue dashed line corresponds to (b). For the blue line, the curves of 3 and four modes are almost equal on the border of 1BZ. On the drawings (a) and (b), the blue surface represents the acoustic mode, while the fuchsia, green, and red surfaces represent the optical CTP modes.
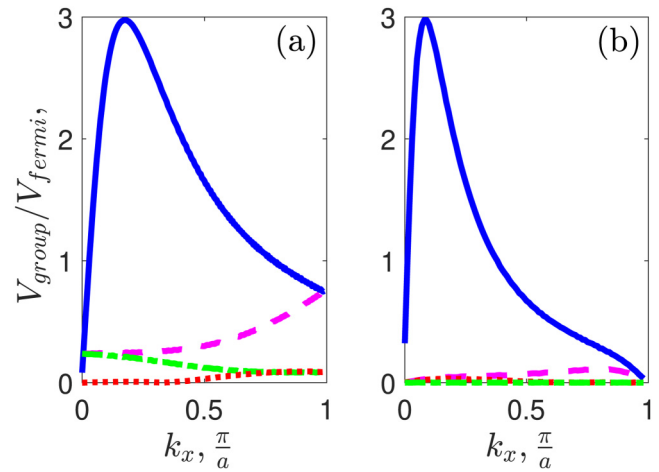

FIG. 5. Dependence of the ratio of plasmon group velocity $V_{group}(\vec{k})$ to electron velocity V_{fermi} on the wave vector k_x. (a) for the chain of four NPs on graphene and (b) for the square structure of four NPs on graphene. The blue curve represents the "acoustic" mode, while the fuchsia dashed, green dash-dotted, and red dotted curves represent the "optical" modes.

parameters of the chain structure $a = b = 4\,\text{R}$ were taken the same as in the experiment in Fig. 1, indicated by a dark green line. One can see very close agreement with the experiment. The slight discrepancy between CTP frequencies calculated by our model and the experiment can be explained by two factors: (1) in the experiment, it were used nanocylinders, while the spherical NPs were used in the model; (2) in the experiment, it was investigated the system consisting of metal nanocylinders on the graphene sheet,
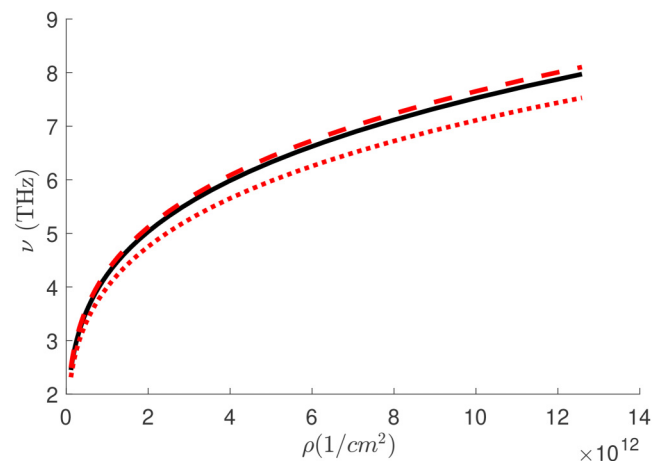

FIG. 6. Calculated CTP frequencies of the NP–graphene systems, plotted as a function of carrier density ρ in graphene. The black solid line corresponds to the highest mode of the chain structure. Red dashed and dotted lines correspond to two higher modes of the square structure.
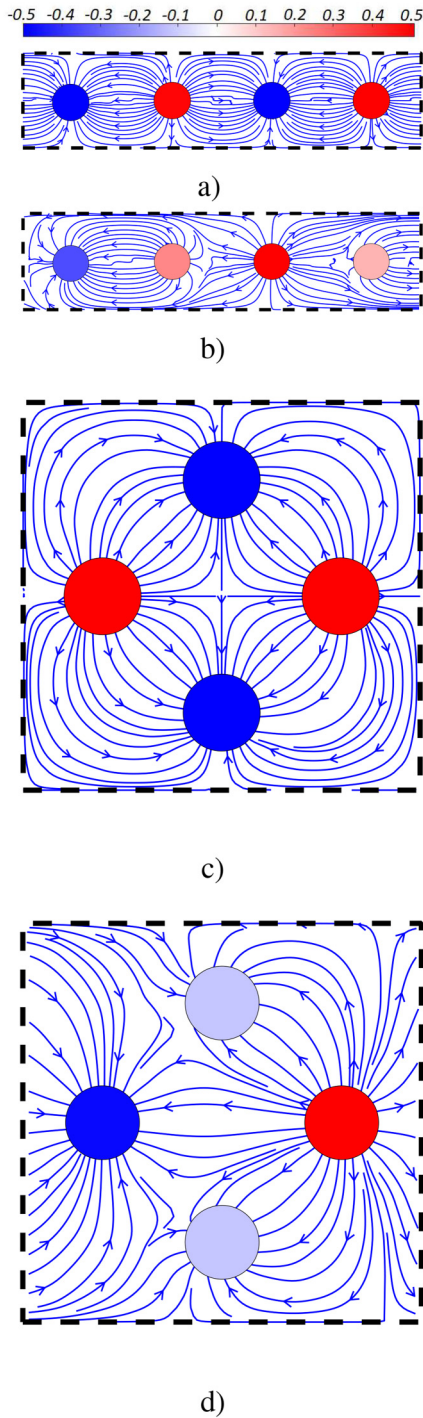
07 August 2024 13:54:35

FIG. 7. Distribution of electric field lines for both structures at different wave vectors k_x. The color and saturation of balls reflect the distribution of effective oscillating NP charges: negative charges are blue and positive charges are red. (a) The chain structure with $k_x = 0$, (b) with $k_x = 0.5 \, \pi/a$. (c) The square structure with $k_x = 0$, (d) with $k_x = 0.5 \, \pi/a$.

under which, instead of a vacuum, a thin layer of SiO$_2$ and a substrate of p-doped silicon were placed, so (16) had to be modified by analogy with (2) from[21]

$$\tilde{\omega}_i^2(\vec{k}) = \omega_i^2(\vec{k})\sqrt{\frac{2}{(1 + \varepsilon_{r_1})}},$$

where the effective permittivity of the underlying medium ε_{r_1} is defined as the weighted average of permittivity of these materials, calculated using the relative weights determined by the overlap factors of the plasmon field intensity distribution with these two materials.

In addition, we plotted the distribution of electric field lines for both investigated structures at different wave vectors k_x and $k_y = 0$ (see Fig. 7). These lines were calculated from the formula $\vec{E}(\vec{r}) = -\nabla \varphi(r) = -\sum_G i\vec{G} \, \varphi(G) \, e^{-i\vec{G}\vec{r}}$. Based on the distribution of the electric field lines and NP charge amplitudes, it can be seen that for the case $k_x = 0$, the distribution of NP charges and field lines is completely symmetrical. This results in a zero dipole moment $P = 0$ of the system. For the case $k_x = 0.5 \, \pi/a$, the distribution of NP charges and the field lines is asymmetrical and this leads to $P \neq 0$. As was shown in Ref. 35, the interaction of an external electromagnetic field (EEF) with a system is determined by the dipole moment P. Consequently, the interaction of EEF with our system will occur only in the case of $k_x = 0.5 \, \pi/a$.

IV. CONCLUSIONS

In this work, we extend the original hybrid quantum-classical model[35] to predict the CTP plasmon properties for the periodical NP arrays on the graphene surface. The linear equations describing the CTP frequencies and eigenvectors (oscillating NP charge values) are derived. It is shown that the CTP plasmon band structure $\omega(\vec{k}, n)$ is characterized by the plasmon wave vectors $\vec{k}$ and the band indexes n, wherein the CTP bands are divided into the acoustic and optical modes, similar to phonons in periodic media. It is demonstrated that these plasmon frequencies lie in the THz range and are factorized, i.e., presented as a product of the factor determined by the graphene charge density and the factor determined by the NP geometry.

The model is applied to two cases of regular NP arrays. In the first case, it is used the chain of four uniformly spaced identical NPs, which, due to identical distances between NPs, can be reduced to the UC containing the single NP only. In the second case, we calculated the CTPs for the periodic structure where the UC contains a square of four same NPs, which cannot be reduced to the smaller one.

In the both cases, the plasmon group velocities $V_{group}(\vec{k})$ tend to zero at $\vec{k} \to 0$ for the acoustic modes but attain their maximum values of $\sim V_{Fermi}$ inside 1BZ. In both cases, the optical modes have weak $\omega(\vec{k}, n)$ dispersion. It is shown that the calculated dependence of CTP frequencies on carrier concentration in graphene is in good agreement with available experimental data.

We believe that the results of this study can help in designing various nanoplasmonic devices operating in the THz range because the developed model makes it possible to carry out CTP

simulations 3–4 orders faster than usually used FEM or FDTD calculations, raising possibilities for predicting the plasmonic properties of very large systems.

AUTHOR DECLARATIONS

Conflict of Interest

The authors have no conflicts to disclose.

Author Contributions

A. S. Fedorov: Conceptualization (equal); Data curation (equal); Funding acquisition (equal); Investigation (equal); Methodology (equal); Project administration (equal); Resources (equal); Supervision (equal); Validation (equal); Writing – original draft (equal); Writing – review & editing (equal). **E. V. Eremkin:** Formal analysis (equal); Investigation (equal); Methodology (equal); Software (equal); Visualization (equal); Writing – original draft (equal).

DATA AVAILABILITY

The data that support the findings of this study are available from the corresponding author upon reasonable request.

REFERENCES

[1]M. Tonouchi, "Cutting-edge terahertz technology," Nat. Photonics **1**(2), 97–105 (2007).

[2]P. Jepsen, D. Cooke, and M. Koch, "Terahertz spectroscopy and imaging—Modern techniques and applications," Laser Photonics Rev. **5**(1), 124–166 (2010).

[3]X. Yang, X. Zhao, K. Yang, Y. Liu, Y. Liu, W. Fu, and Y. Luo, "Biomedical applications of terahertz spectroscopy and imaging," Trends Biotechnol. **34**(10), 810–824 (2016).

[4]V. Ryzhii, M. Ryzhii, V. Mitin, and M. S. Shur, "Graphene tunneling transit-time terahertz oscillator based on electrically induced p–i–n junction," Appl. Phys. Express **2**, 034503 (2009).

[5]N. M. Burford and M. O. El-Shenawee, "Review of terahertz photoconductive antenna technology," Opt. Eng. **56**(1), 010901 (2017).

[6]F. H. L. Koppens, D. E. Chang, and F. J. G. de Abajo, "Graphene plasmonics: A platform for strong light–matter interactions," Nano Lett. **11**(8), 3370–3377 (2011).

[7]T. Low and P. Avouris, "Graphene plasmonics for terahertz to mid-infrared applications," ACS Nano **8**(2), 1086–1101 (2014).

[8]P. Tassin, T. Koschny, and C. M. Soukoulis, "Graphene for terahertz applications," Science **341**(6146), 620–621 (2013).

[9]A. Tredicucci and M. S. Vitiello, "Device concepts for graphene-based terahertz photonics," IEEE J. Sel. Top. Quantum Electron. **20**(1), 130–138 (2014).

[10]W. Gao, G. Shi, Z. Jin, J. Shu, Q. Zhang, R. Vajtai, P. M. Ajayan, J. Kono, and Q. Xu, "Excitation and active control of propagating surface plasmon polaritons in graphene," Nano Lett. **13**(8), 3698–3702 (2013).

[11]X. Zhu, W. Yan, P. U. Jepsen, O. Hansen, N. A. Mortensen, and S. Xiao, "Experimental observation of plasmons in a graphene monolayer resting on a two-dimensional subwavelength silicon grating," Appl. Phys. Lett. **102**(13), 131101 (2013).

[12]S. Zou, N. Janel, and G. C. Schatz, "Silver nanoparticle array structures that produce remarkably narrow plasmon lineshapes," J. Chem. Phys. **120**(23), 10871–10875 (2004).

[13]D. Khlopin, F. Laux, W. P. Wardley, J. Martin, G. A. Wurtz, J. Plain, N. Bonod, A. V. Zayats, W. Dickson, and D. Gérard, "Lattice modes and plasmonic linewidth engineering in gold and aluminum nanoparticle arrays," J. Opt. Soc. Am. B **34**(3), 691 (2017).

[14]M. S. Bin-Alam, O. Reshef, Y. Mamchur, M. Z. Alam, G. Carlow, J. Upham, B. T. Sullivan, J. -M. Ménard, M. J. Huttunen, R. W. Boyd, and K. Dolgaleva, "Ultra-high-q resonances in plasmonic metasurfaces," Nat. Commun. **12**(1), 974 (2021).

[15]X. Li, X. Xu, H. Zhou, Y. Gu, F. Liu, and W. Wu, "Ultra-broadband tunable terahertz absorber of graphene and hierarchical plasmonic metamaterials," Adv. Devices Instrum. **4**, 0014 (2023).

[16]V. Sorathiya, S. Lavadiya, B. Parmar, S. Das, M. Krishna, O. S. Faragallah, M. Baz, M. M. Eid, and A. N. Z. Rashed, "Numerical investigation of the tunable polarizer using gold array and graphene metamaterial structure for an infrared frequency range," Appl. Phys. B **128**, 1–9 (2022).

[17]H. Wang, J. Linghu, X. Wang, Q. Zhao, and H. Shen, "Angular-dependent Thz modulator with hybrid metal-graphene metastructures," Nanomaterials **13**(13), 1914 (2023).

[18]Y. Liu, R. Zhong, J. Huang, Y. Lv, C. Han, and S. Liu, "Independently tunable multi-band and ultra-wide-band absorbers based on multilayer metal-graphene metamaterials," Opt. Express **27**(5), 7393–7404 (2019).

[19]A. B. Shruti and S. Pahadsingh, "Quad-band graphene-based terahertz metamaterial perfect absorber for refractive index sensing," Plasmonics **17**(6), 2323–2336 (2022).

[20]J.-X. Wu, X.-H. Deng, H.-F. Liu, and J. Yuan, "Perfect terahertz absorber with dynamically tunable peak and bandwidth using graphene-based metamaterials," JOSA B **39**(9), 2313–2318 (2022).

[21]K. Tantiwanichapan, X. Wang, H. Durmaz, Y. Li, A. K. Swan, and R. Paiella, "Graphene terahertz plasmons: A combined transmission spectroscopy and Raman microscopy study," ACS Photonics **4**(8), 2011–2017 (2017).

[22]E. H. Hwang, S. Adam, and S. D. Sarma, "Carrier transport in two-dimensional graphene layers," Phys. Rev. Lett. **98**(18), 186806 (2007).

[23]A. Yariv and P. Yeh, *Optical Waves in Crystals: Propagation and Control of Laser Radiation*, Wiley Classics Library (Wiley-Interscience, 2003).

[24]A. Taflove and M. E. Brodwin, "Numerical solution of steady-state electromagnetic scattering problems using the time-dependent Maxwell's equations," IEEE Trans. Microwave Theory Tech. **23**(8), 623–630 (1975).

[25]K. Yee, "Numerical solution of initial boundary value problems involving Maxwell's equations in isotropic media," IEEE Trans. Antennas Propag. **14**(3), 302–307 (1966).

[26]Y. Cai, J. Zhu, and Q. H. Liu, "Tunable enhanced optical absorption of graphene using plasmonic perfect absorbers," Appl. Phys. Lett. **106**(4), 043105 (2015).

[27]Y. Xiang, X. Dai, J. Guo, H. Zhang, S. Wen, and D. Tang, "Critical coupling with graphene-based hyperbolic metamaterials," Sci. Rep. **4**(1), 5483 (2014).

[28]Y. Zhang, Y. Feng, B. Zhu, J. Zhao, and T. Jiang, "Graphene based tunable metamaterial absorber and polarization modulation in terahertz frequency," Opt. Express **22**(19), 22743 (2014).

[29]A. Fedorov, P. Krasnov, M. Visotin, F. Tomilin, S. Polyutov, and H. Ågren, "Charge-transfer plasmons with narrow conductive molecular bridges: A quantum-classical theory," J. Chem. Phys. **151**(24), 244125 (2019a).

[30]A. Fedorov, M. Visotin, V. Gerasimov, S. Polyutov, and P. Avramov, "Charge transfer plasmons in the arrays of nanoparticles connected by conductive linkers," J. Chem. Phys. **154**(8), 084123 (2021).

[31]A. S. Fedorov, M. A. Visotin, E. V. Eremkin, P. O. Krasnov, H. Ågren, and S. P. Polyutov, "Charge-transfer plasmons of complex nanoparticle arrays

connected by conductive molecular bridges," Phys. Chem. Chem. Phys. **24**(32), 19531–19540 (2022).

[32]A. S. Fedorov, P. O. Krasnov, M. A. Visotin, F. N. Tomilin, S. P. Polyutov, and H. Ågren, "Charge-transfer plasmons with narrow conductive molecular bridges: A quantum-classical theory," J. Chem. Phys. **151**, 244125 (2019b).

[33]S. Datta, *Electronic Transport in Mesoscopic Systems* (Cambridge University Press, 1995).

[34]L. D. Landau and L. P. Pitaevskii, in *Electrodynamics of Continuous Media*, 2nd edition, Course of Theoretical Physics (Butterworth-Heinemann, Oxford, 1984)

[35]A. S. Fedorov, E. V. Eremkin, P. O. Krasnov, V. S. Gerasimov, H. Ågren, and S. P. Polyutov, "A hybrid quantum–classical theory for predicting terahertz charge-transfer plasmons in metal nanoparticles on graphene," J. Chem. Phys. **160**(4), 044117 (2024).

07 August 2024 13:54:35